Electronic structure and transport anisotropy of Bi₂Te₃ and Sb₂Te₃

B. Yu. Yavorsky,[1,*] N. F. Hinsche,[1] I. Mertig,[1,2] and P. Zahn[1]

[1]*Institut für Physik, Martin-Luther-Universität Halle-Wittenberg, D-06099 Halle, Germany*
[2]*Max-Planck-Institut für Mikrostrukturphysik, Weinberg 2, D-06120 Halle, Germany*

On the basis of detailed *ab initio* studies, the influence of strain on the anisotropy of the transport distribution of the thermoelectrics Bi₂Te₃ and Sb₂Te₃ was investigated. Both tellurides were studied in their own as well as in their copartner's lattice structure to gain insight into the electrical transport in epitaxial heterostructures composed of both materials. It is shown that the anisotropy of the transport distribution overestimates the experimental findings for Bi₂Te₃, implying anisotropic scattering effects. An increase of the in-plane lattice constant leads to an enhancement of the transport anisotropy for *p* doping, whereas the opposite occurs for *n* doping. The recent findings and special features of the transport distribution are discussed in detail in relation to the topology of the band structures.

PACS number(s): 71.15.Mb, 71.15.Rf, 71.20.Nr, 72.20.Pa

I. INTRODUCTION

Thermoelectric (TE) materials have huge potential for power generation, heat pumping, and refrigeration. However, their practical application is restricted because of the low performance of the TE devices compared to traditional fossil-fuel power generators and compressor-based refrigerators.[1] A high-performance TE material has to be a good electrical conductor as well as a poor thermal conductor and, at the same time, possess a large Seebeck coefficient.[2] Quantitatively, the efficiency of TE devices is expressed by the dimensionless figure of merit ZT,

$$ZT = \alpha^2 \sigma T / (\kappa_L + \kappa_e), \tag{1}$$

where α, σ, and T are the Seebeck coefficient, electrical conductivity, and absolute temperature, and κ_L, κ_e are phonon and electron contributions to the total thermal conductivity, respectively.

Bismuth and antimony tellurides, Bi₂Te₃ and Sb₂Te₃, and the alloys based on these materials play a significant role in thermoelectric technology. Early studies of the (Bi$_x$,Sb$_{2-x}$)Te₃ compounds in the late 1950s already reported $ZT \sim 1$ at room temperature,[3] which was confirmed by further experiments.[4] This value remains, even to date, the maximal one available at room temperature for bulk materials. Current progress in nanostructure fabrication, in particular the epitaxial growth of high-quality superlattices,[5] encourages the possibility of significant performance improvement of TE devices. Venkata-subramanian *et al.* reported $ZT \sim 2.4$ and $ZT \sim 1.45$ at 300 K for *p*-type and *n*-type Bi₂Te₃/Sb₂Te₃ superlattices, respectively.[6]

These experimental advances motivated extensive theoretical studies of the electronic structure of the bulk bismuth and antimony telluride aimed toward understanding the possible origin of the increased thermoelectic performance in the multi-layered structures. While in previous years only a few *ab initio* band-structure calculations of the bulk bismuth telluride[7,8] could be mentioned, in the last decade various aspects of the electronic structure of both pure and doped bulk Bi₂Te₃ and Sb₂Te₃, as well as their transport properties, were discussed in Refs. 9–21. *Ab initio* studies of the electronic structure and the

transport properties of Bi₂Te₃/Sb₂Te₃ superlattices were also reported.[22]

An explanation of directional anisotropy of the transport properties in Bi₂Te₃/Sb₂Te₃ superlattices could play a crucial role in the understanding of their increased figure of merit. Venkatasubramanian *et al.*[6] found a strong dependence of the anisotropy of the carrier mobility on both the superlattice period and the relative thickness of the constituents. The enhancement of the electrical conductivity parallel to the epitaxial growth direction, i.e., the trigonal axis of the rhombohedral lattice of bismuth and antimony tellurides, together with the possibility to suppress the lattice thermal conductivity κ_L along this direction, could provide the desirable ZT enhancement. It is reasonable to assume that the epitaxial growth of the layered structures affects essentially the out-of-plane transport compared to the bulk constituents. Therefore, the synthesis of the high-performance thermoelectric materials should, among others, provide a decrease of the in-plane versus out-of-plane current anisotropy.

In this study, we concentrate on the anisotropy of the transport properties in the bulk Bi₂Te₃ and Sb₂Te₃ as a first step toward understanding the corresponding properties of the Bi₂Te₃/Sb₂Te₃ superlattices. Since epitaxial growth always implies lattice distortions, we included, as discussed below, the effect of the lattice relaxation in our study.

II. CRYSTAL STRUCTURE

Both bismuth and antimony telluride possess the rhombohedral crystal structure with five atoms, i.e., one formula unit per unit cell belonging to the space group D_{3d}^5 ($R\bar{3}m$). The experimental lattice parameters[23] are $a_{\mathrm{BiTe}}^{\mathrm{rh}} = 10.473$ Å, $\theta_{\mathrm{BiTe}} = 24.17°$, and $a_{\mathrm{SbTe}}^{\mathrm{rh}} = 10.447$ Å, $\theta_{\mathrm{SbTe}} = 23.55°$, where θ is the angle between the rhombohedral basis vectors of the length a^{rh}. In order to emphasize the layered character of this structure, it is convenient to rearrange it into the hexagonal unit cell built up by three formula units, as shown in Fig. 1. The hexagonal cell contains 15 atoms grouped in the three "quintuple" layers, Te1-Bi(Sb)-Te2-Bi(Sb)-Te1, where Te1 and Te2 are two different crystal types of tellurium atoms. The "hexagonal" lattice parameters are $a_{\mathrm{BiTe}}^{\mathrm{hex}} = 4.384$ Å, $c_{\mathrm{BiTe}}^{\mathrm{hex}} = 30.487$ Å, and $a_{\mathrm{SbTe}}^{\mathrm{hex}} = 4.264$ Å, $c_{\mathrm{SbTe}}^{\mathrm{hex}} = 30.458$ Å, for Bi₂Te₃
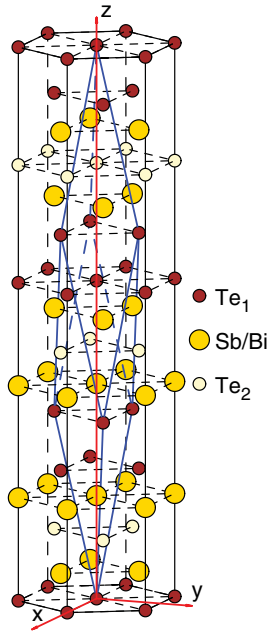
FIG. 1. (Color online) The rhombohedral unit cell superimposed with the hexagonal one to emphasize the layered character of the material.

and Sb_2Te_3, respectively. In bismuth telluride, the nearest interatomic distances between the individual monolayers inside the quintuple blocks are 3.07 Å for Te1-Bi and 3.25 Å for Bi-Te2. Two adjacent quintuple layers in Bi_2Te_3 are separated by a somewhat longer distance, 3.63 Å for Te1-Te1. In the antimony telluride, these distances are 2.98 Å for Te1-Sb, 3.17 Å for Sb-Te2 inside the quintuple blocks, and 3.74 Å for Te1-Te1 between the blocks.

In the Bi_2Te_3/Sb_2Te_3 multilayers, atoms change their bulk positions due to the mismatch of the lattice parameters. The description of the realistic crystal structure of the multi-layers is beyond the scope of this study. Nonetheless, we modeled Bi_2Te_3 with the experimental lattice parameters and interatomic distances of Sb_2Te_3, and vice versa. Since both materials have very similar lattice parameter c^{hex} along the z axis, this variation is essentially compression and extension of the lattice in the xy plane for bismuth and antimony telluride, respectively. We assume that one could estimate the effect of the lattice relaxation on the electronic and transport properties in the Bi_2Te_3/Sb_2Te_3 heterostructures from these two limiting cases.

III. CALCULATIONAL DETAILS

Calculations of the electronic structures were performed by means of the screened Korringa-Kohn-Rostoker (KKR) Green's function method[24] in the atomic sphere approximation (ASA) within the local density approximation of the density functional theory in the parametrization of Vosko et al.[25] The angular momentum expansion was cut off at $l_{max} = 3$. It is generally recognized that the effects of spin-orbit coupling are mandatory for the correct treatment of the band structure in these materials. Therefore, we used a fully relativistic version of the method based on the Dirac equation.[26] The obtained

self-consistent band structures were used for the calculations of the transport distribution $\sigma_{\alpha\beta}$ within the Boltzmann formalism, assuming a constant relaxation time τ,[27]

$$\sigma_{\alpha\beta}(E) = \tau \frac{e^2}{(2\pi)^3\hbar} \sum_j \int_{\varepsilon^j(\mathbf{k})=E} dS \frac{v_\alpha^j(\mathbf{k})v_\beta^j(\mathbf{k})}{|\mathbf{v}^j(\mathbf{k})|},$$

$$\mathbf{v}^j(\mathbf{k}) = \frac{1}{\hbar} \nabla_\mathbf{k} \varepsilon^j(\mathbf{k}),$$

(2)

where $\varepsilon^j(\mathbf{k})$ is the jth band energy at the $\mathbf{k}$-point of the Brillouin zone (BZ), and α and β denote Cartesian coordinates. In this approach, the carrier-scattering probability is averaged over the initial and final states, and is independent of a specific scattering mechanism. This assumption is reliable as far as the electronic band-structure effects on the transport properties are concerned.

In layered systems, the relaxation time is, in general, anisotropic. In particular, Ashworth et al.[28] extracted the values of $\tau_{xx}/\tau_{zz} \sim 2$ in both n- and p-doped Bi_2Te_3 at small carrier concentrations from the galvanomagnetic and de Haas-van Alphen measurements.[29] With an increase of the carrier concentration, the anisotropy of the relaxation time decays smoothly. The exact behavior of this decay depends on a type of carrier scattering in the material, and should not be affected by a small symmetry-conserving lattice strain. The total transport anisotropy includes the band-structure contribution modulated by the relaxation-time anisotropy. However, the sense of the change, i.e., increase or decrease, due to the small lattice strain should not be influenced by this modulation. Therefore, we assume the relaxation time to be isotropic. In this approximation, the transport anisotropy ratio σ_{xx}/σ_{zz} is independent of the relaxation time, and we do not have to specify it.

The $\mathbf{k}$-space integration over the isoenergetic surfaces was performed using the tetrahedron method on the Blöchl mesh[33] of $96 \times 96 \times 96$ points in the whole BZ. In the energy intervals of the width about 0.1 eV in the vicinity of both band edges, the integration was refined by means of an adaptive mesh up to $4 \times 4 \times 4$ times as dense as the original one. As a convergence criterium, we used the values of the transport anisotropy ratio calculated from the effective mass approximation at the band extrema.[30]

IV. ELECTRONIC STRUCTURES AND TRANSPORT PROPERTIES

The electronic band structures for Bi_2Te_3 and Sb_2Te_3 for both experimental and strained lattices are shown in Fig. 2. The positions of the high-symmetry points in the BZ of the rhombohedral structure are denoted in Fig. 3. Our results at the experimental lattice parameters agree well with the previous *ab initio* studies of Mishra et al.,[8] Larson et al.[9] for Bi_2Te_3, and Eremeev et al.[21] for both Bi_2Te_3 and Sb_2Te_3. At the same time, the calculations made with the full-potential linearized augmented plane-wave (FLAPW) method result in slightly different band structures for the bismuth and antimony tellurides at both the experimental[10–13,19] and strained[18,20] lattices. The key question of the band structure of Bi_2Te_3 and Sb_2Te_3 is the position of the valence-band maximum
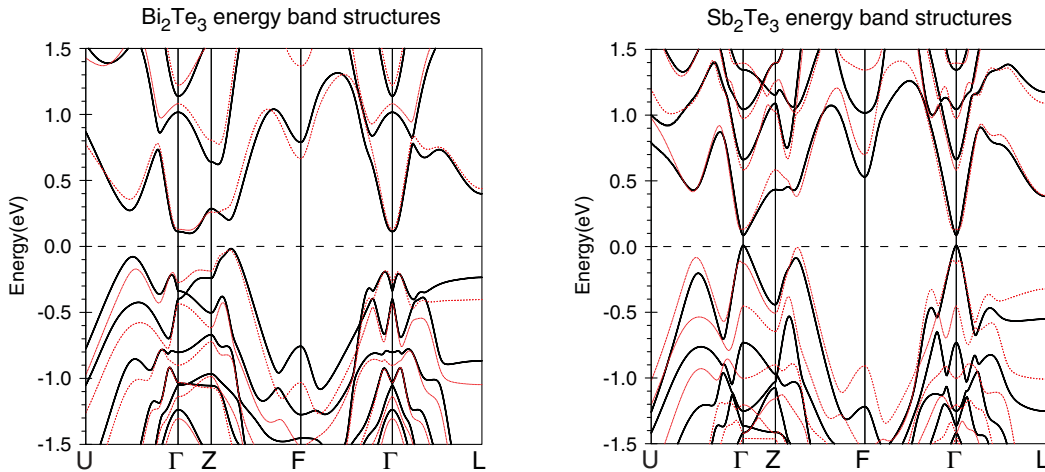
FIG. 2. (Color online) Band structures of Bi_2Te_3 and Sb_2Te_3 along symmetry lines for both experimental (solid lines) and strained (dashed lines) lattices. Energies are given relative to the VBM.

(VBM) and conduction-band minimum (CBM) in the BZ. The calculations of Refs. 10–13 and 19 result in both a six-valley VBM and CBM located in the symmetry plane (ΓZU), in agreement with experiments for both the bismuth[31] and antimony[32] tellurides. Unlike these results, in our case the CBM of Bi_2Te_3 at both lattice parameters, a_{BiTe} and a_{SbTe}, is a two-valley minimum located on the symmetry line ΓZ, similarly to Ref. 8. Our calculations also detected the six-valley local conduction-band minimum (LCBM) that occurred in the plane (ΓZU), however, at slightly higher energy. For Sb_2Te_3 at the experimental lattice parameters, we found a direct band gap located at the center of the BZ, while at the larger in-plane lattice constant, both the six-valley VBM and CBM lie in the symmetry plane (ΓZU). The electronic structures of Bi_2Te_3 and Sb_2Te_3 near the band gap at $a = a_{BiTe}$ along the lines connecting band extrema in the symmetry plane (ΓZU) are shown in Fig. 4. In contrast to our results, Thonhauser[14] found that the increase of the lattice parameters in Sb_2Te_3 led to the formation of a direct band gap at the Γ point. On the other hand, the negative hydrostatic pressure discussed in Ref. 14 implies an increase of both in-plane and out-of-plane lattice parameters in comparable degree, while in our study essentially the first one is included. Additionally, calculations in Ref. 14 were performed for optimized atomic positions with respect to the total energy, which can affect the band structure of antimony telluride.[18]

As already discussed,[8,10] these differences in the band structures are probably due to the nonspherical part of the potential, which is not included in the ASA. At the same time, as discussed below, these differences have no significant
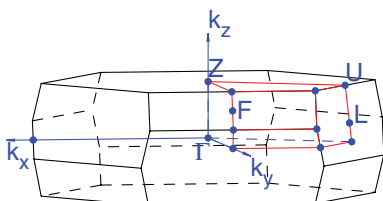
impact on the transport distribution, $\sigma(E)$. The details of the band structures for all four systems are compiled in Table I.

The calculated transport distribution of Bi_2Te_3 at both the experimental ($a = a_{BiTe}$) and compressed ($a = a_{SbTe}$) lattice parameters are shown in Fig. 5 together with the anisotropy ratio, σ_{xx}/σ_{zz}. In terms of the rigid band model, the energies below and above the band gap simulate p and n doping, respectively. While for p doping close to the VBM, σ_{xx}/σ_{zz} varies smoothly approaching the limiting value, the ratio increases drastically and forms a prominent two-peak structure for the n-doping case. This structure originates from the two topological transformations of the constant energy surfaces in the conduction band. Figure 6(a) shows the contour plot of $\varepsilon(\mathbf{k})$ for Bi_2Te_3 at $a = a_{BiTe}$ in the plane (ΓZU) for energies 0 to 0.19 eV relative to the conduction band edge. The main features of the band structure are the global CBM on the line ΓZ, the LCBM at (0.666, 0.602, 0.602), and the two saddle points, s_1 at (0.722, 0.667, 0.667) and s_2 at (0.493, 0.461, 0.461), in crystallographic coordinates. The saddle point s_1 occurs at $E - E_{CBM} = 0.05$ eV and causes the first peak of σ_{xx}/σ_{zz}, while s_2 appears at 0.17 eV and forms the second peak. At room temperature, the chemical potential would be located in the saddle point s_1 or s_2, for an electron carrier concentration of about $N = 3.0 \times 10^{19}$ cm^{-3} or $N = 1.5 \times 10^{20}$ cm^{-3}, respectively.

Now we address the question of whether the electronic structure of Bi_2Te_3 with the six-valley CBM reported in Refs. 10–13,18, and 19 would result in a significantly different transport anisotropy near the band gap for n doping. The six-valley conduction band structure can be approximately modeled from the two-valley one detected in our KKR-ASA calculation by an energy shift of $\sim$0.04 eV downward and upward for the LCBM and CBM, respectively [see Fig. 4(a)]. This model band structure would have a limiting value of $\sigma_{xx}/\sigma_{zz} = 4.95$ at the conduction-band edge as calculated from the effective mass approximation at the LCBM, which is fairly close to 4.7 at the CBM. Since the saddle point s_1 lies close to the line connecting the CBM and LCBM, the relative shift of the minima would not affect remarkably its energy position, and the model band structure would also result in a

FIG. 3. (Color online) Brillouin zone of the rhombohedral lattice.

TABLE I. Band-structure parameters: Band gap in eV, positions of VBM and CBM in crystallographic coordinates, effective masses in electron mass units, principal axes $\mathbf{e}_i$ in Cartesian coordinates, and transport anisotropy ratio from the effective mass approximation.

	$\mathrm{Bi_2Te_3}$			
Lattice parameters	$a = a_{\mathrm{BiTe}}$		$a = a_{\mathrm{SbTe}}$	
Gap (eV)	0.105		0.129	
Extremum	VBM	CBM	VBM	CBM
Position	0.517 0.366 0.366	0.173 0.173 0.173	0.405 0.405 0.335	0.151 0.151 0.151
Effective masses				
m_1	-0.024	0.178	-0.039	0.154
m_2	-0.134	0.178	-0.077	0.154
m_3	-1.921	0.835	-0.207	1.370
Principal axes				
$\mathbf{e}_1$	$0.500 -0.867\ 0.000$	$1.000\ 0.000\ 0.000$	$0.866\ 0.499 -0.024$	$1.000\ 0.000\ 0.000$
$\mathbf{e}_2$	$0.600\ 0.346\ 0.721$	$0.000\ 1.000\ 0.000$	$0.500 -0.867\ 0.000$	$0.000\ 1.000\ 0.000$
$\mathbf{e}_3$	$0.625\ 0.361 -0.693$	$0.000\ 0.000\ 1.000$	$0.021\ 0.012\ 0.999$	$0.000\ 0.000\ 1.000$
σ_{xx}/σ_{zz}	5.452	4.700	4.020	9.013
	$\mathrm{Sb_2Te_3}$			
Lattice parameters	$a = a_{\mathrm{SbTe}}$		$a = a_{\mathrm{BiTe}}$	
Gap (eV)	0.090		0.140	
Extremum	VBM	CBM	VBM	CBM
Position	0.000 0.000 0.000	0.000 0.000 0.000	0.547 0.392 0.392	0.004 0.020 0.020
Effective masses				
m_1	-0.054	0.045	-0.039	1.124
m_2	-0.054	0.045	-0.083	1.774
m_3	-0.102	0.114	-2.046	6.861
Principal axes				
$\mathbf{e}_1$	$1.000\ 0.000\ 0.000$	$1.000\ 0.000\ 0.000$	$0.500 -0.867\ 0.000$	$-0.316 -0.183\ 0.931$
$\mathbf{e}_2$	$0.000\ 1.000\ 0.000$	$0.000\ 1.000\ 0.000$	$0.594\ 0.343\ 0.727$	$0.500 -0.867\ 0.000$
$\mathbf{e}_3$	$0.000\ 0.000\ 1.000$	$0.000\ 0.000\ 1.000$	$0.630\ 0.363 -0.686$	$0.806\ 0.465\ 0.365$
σ_{xx}/σ_{zz}	1.889	2.507	2.397	2.080

peak of σ_{xx}/σ_{zz} at $\sim$0.05 eV relative to the conduction-band edge. As we already discussed, the second peak in the transport anisotropy at $E - E_{\mathrm{CBM}} = 0.17$ eV occurs from the saddle point s_2 close to the local band maximum at Z. This topological feature was detected both in the FLAPW[10–13,18,19] method and in our KKR-ASA calculations. Based on this consideration, we expect that the transport anisotropy of the bismuth telluride at the experimental lattice parameters is stable with respect to a slight modification between the two-valley and six-valley conduction bands.

In $\mathrm{Bi_2Te_3}$, the in-plane compression of the lattice parameters from $a = a_{\mathrm{BiTe}}$ to $a = a_{\mathrm{SbTe}}$ increases the transport anisotropy ratio at the conduction-band edge remarkably. Within the effective mass approximation, this can be explained by the enhancement of the ratio $m_\perp/m_\parallel$ due to the expansion of the BZ in the xy plane. At the same time, σ_{xx}/σ_{zz} decreases at the valence-band edge. In this case, the compression of the lattice results in a reorientation of the longest axis of the effective mass ellipsoid near the VBM closer to the z axis, which leads to an increase of the transport anisotropy
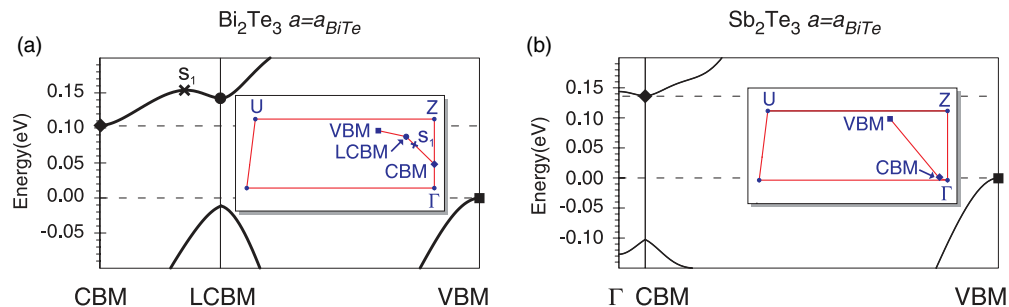

FIG. 4. (Color online) Band structures of (a) $\mathrm{Bi_2Te_3}$ and (b) $\mathrm{Sb_2Te_3}$ at $a = a_{\mathrm{BiTe}}$ near the band gap along the lines shown in the insets.
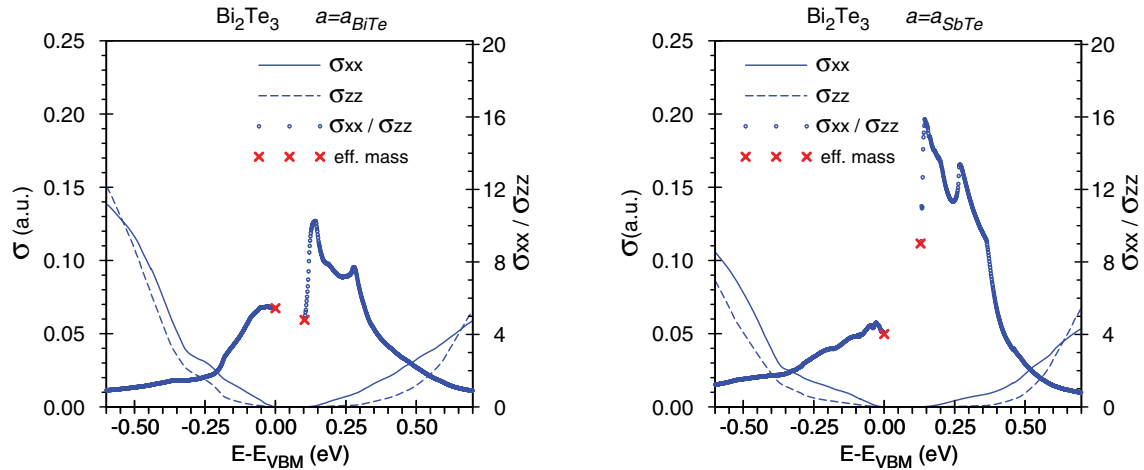
FIG. 5. (Color online) Transport distribution $\sigma_{xx}(E)$ and $\sigma_{zz}(E)$ and the transport anisotropy σ_{xx}/σ_{zz} for Bi_2Te_3 at the experimental and compressed lattice parameters. Crosses at the band edges mark the σ_{xx}/σ_{zz} ratio derived from the effective mass model[30] using the parameters of Table I.

ratio, and at the same time decreases the anisotropy of the dominating effective masses m_2 and m_3 (see Table I). The last effect prevails over the enhancement of σ_{xx}/σ_{zz} due to the rotation of the effective mass ellipsoid.

Figure 7 shows the transport distribution and the anisotropy ratio of Sb_2Te_3 at both $a = a_{SbTe}$ and $a = a_{BiTe}$. The kink of the anisotropy ratio at the experimental lattice parameters is induced by the saddle point $s = (0.831, 0.784, 0.784)$ at $E - E_{VBM} = 0.116$ eV, which corresponds to a hole carrier concentration of $N = 5.8 \times 10^{19}$ cm^{-3} at 300 K. This topology is illustrated in Fig. 6(b), which shows the contour plot of $\varepsilon(\mathbf{k})$ in the valence band of the antimony telluride for energies -0.24 to 0 eV relative to E_{VBM}. The in-plane expansion of the lattice parameter increases the density of the occupied states near the valence-band edge and suppresses the kink. The transport anisotropy ratio increases with the in-plane

compression of the BZ at the valence-band edge, and, at the same time, decreases at the conduction-band edge due to the larger angle between the z axis and the largest axis of the effective mass ellipsoid, similarly to the discussed changes in bismuth telluride.

Now we discuss the effect of the lattice strain on the in-plane and out-of-plane transport separately. In bismuth telluride, the enhancement of the anisotropy ratio σ_{xx}/σ_{zz} at the conduction-band edge due to the in-plane compression is associated essentially with the decrease of the σ_{zz} component. In particular, the effective mass approximation at the CBM gives the values of $\sigma_{zz}(a_{SbTe})/\sigma_{zz}(a_{BiTe}) = 0.61$ and $\sigma_{xx}(a_{SbTe})/\sigma_{xx}(a_{BiTe}) = 1.15$. At the same time, the reduction of the anisotropy at the valence-band edge is implied by a slight increase of 1.24 times of the out-of-plane component and a decrease of 0.92 times of the in-plane component,
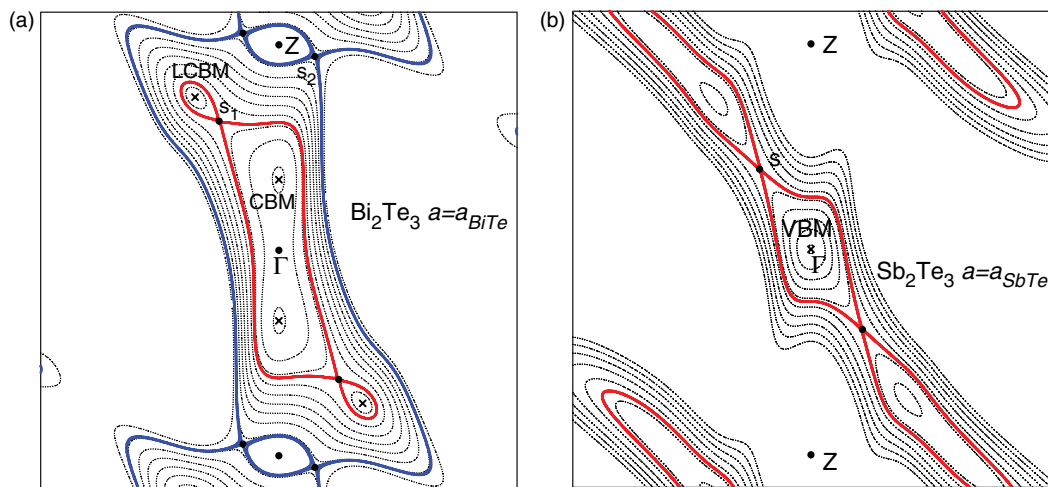

FIG. 6. (Color online) Contour plots of $\varepsilon(\mathbf{k})$ at the experimental lattice constants in the plane $(\Gamma Z U)$. (a) Bi_2Te_3: 10 isolines for $(E - E_{CBM})$ at 0 to 0.19 eV with a constant increment (dotted); additionally, two isolines at $E - E_{CBM} = 0.05$ eV and $E - E_{CBM} = 0.17$ eV with the saddle points s_1 and s_2, respectively (bold). The positions of the CBM and the LCBM are marked with crosses. (b) Sb_2Te_3: 10 isolines for $(E - E_{VBM})$ at -0.24 to 0 eV with a constant increment (dotted); additionally, one isoline with the saddle point s (bold). The position of the VBM is marked with a cross.
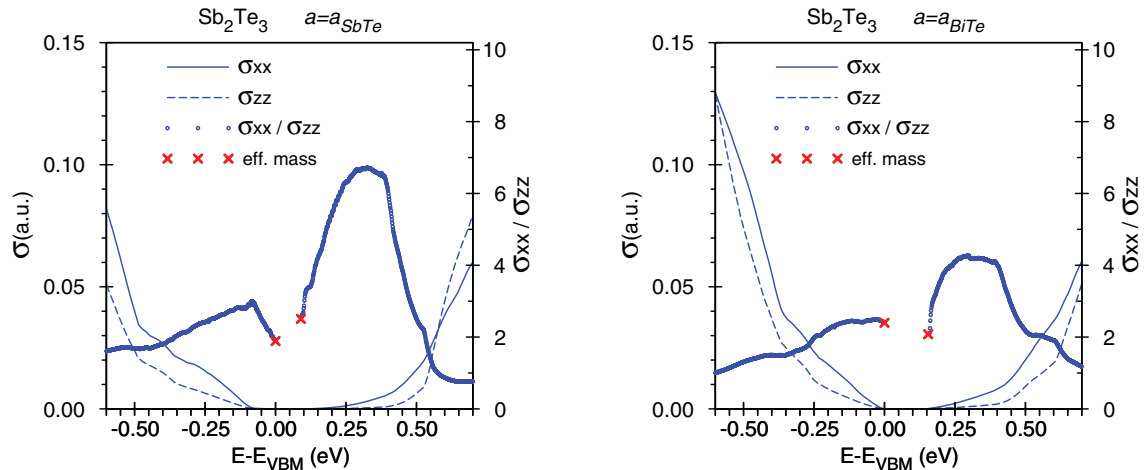
FIG. 7. (Color online) Transport distribution and the transport anisotropy for Sb_2Te_3 at the experimental and expanded lattice parameters. Crosses at the band edges mark the σ_{xx}/σ_{zz} derived from the effective mass model[30] using the parameters of Table I.

respectively. In antimony telluride, the in-plane expansion decreases significantly both the in-plane and out-of-plane transport. At the valence-band edge, the decrease of 0.49 and 0.26 was found within the effective mass model for the in-plane and out-of-plane components, respectively. An even more pronounced decrease of $\sigma_{xx}(a_{BiTe})/\sigma_{xx}(a_{SbTe}) = 0.18$ and $\sigma_{zz}(a_{BiTe})/\sigma_{zz}(a_{SbTe}) = 0.21$ was detected at the conduction-band edge. However, because of the similar rates of decrease for both the in-plane and out-of-plane components, the lattice expansion has only a modest effect on the transport anisotropy ratio σ_{xx}/σ_{zz} in Sb_2Te_3 at both the conduction- and valence-band edges.

V. CONCLUSIONS

On the basis of *ab initio* electronic structures obtained with the fully relativistic KKR method, we studied the anisotropy of the transport properties of the bismuth and antimony tellurides in the constant relaxation-time approximation within the Boltzmann formalism. In addition to the systems with the experimental lattice parameters, we modeled bismuth telluride within the lattice of Sb_2Te_3, and vice versa. We found that

a decrease of the in-plane lattice parameters increases the transport anisotropy for the *n* doping and, at the same time, decreases the anisotropy for the *p*-doped case. In order to estimate the possible influence of the lattice strain on the thermoelectric performance, in particular the out-of-plane current, in Bi_2Te_3/Sb_2Te_3 superlattices, we discussed separately the effect of the in-plane structural relaxation on both the in-plane and out-of-plane transport at the band-gap edges. A slight enhancement of σ_{zz} due to the in-plane expansion was detected for the *p*-doped bismuth telluride. In all other cases, the strain led to a decrease of the out-of-plane component. These effects can be understood within the effective mass approximation at the valence-band maximum and conduction-band minimum, respectively.

---

*bogdan.yavorsky@physik.uni-halle.de

[1] F. J. DiSalvo, Science **285**, 703 (1999).

[2] L. E. Bell, Science **321**, 1457 (2008).

[3] C. B. Satterthwaite and R. W. Ure, Phys. Rev. **108**, 1164 (1957); F. D. Rosi, B. Abeles, and R. S. Jensen, J. Phys. Chem. Solids **10**, 191 (1959).

[4] J. P. Fleurial, L. Gailliard, R. Triboulet, H. Scherrer, and S. Scherrer, J. Phys. Chem. Solids **49**, 1237 (1988); T. Caillat, M. Carle, P. Pierrat, H. Scherrer, and S. Scherrer, *ibid.* **53**, 1121 (1992).

[5] R. Venkatasubramanian, T. Colpitts, B. O'Quinn, S. Liu, N. El-Masry, and M. Lamvik, Appl. Phys. Lett. **75**, 1104 (1999).

[6] R. Venkatasubramanian, E. Siilova, T. Colpitts, and B. O'Quinn, Nature (London) **413**, 597 (2001).

[7] G. A. Thomas, D. H. Rapkine, R. B. Van Dover, L. F. Mettheiss, W. A. Sunder, L. F. Schneemeyer, and J. V. Waszczak, Phys. Rev. B **46**, 1553 (1992).

[8] S. K. Mishra, S. Satpathy, and O. Jepsen, J. Phys. Condens. Matter **9**, 461 (1997).

[9] P. Larson, S. D. Mahanti, and M. G. Kanatzidis, Phys. Rev. B **61**, 8162 (2000).

[10] S. J. Youn and A. J. Freeman, Phys. Rev. B **63**, 085112 (2001).

[11] T. J. Scheidemantel, C. Ambrosch-Draxl, T. Thonhauser, J. V. Badding, and J. O. Sofo, Phys. Rev. B **68**, 125210 (2003).

[12] T. Thonhauser, T. J. Scheidemantel, J. O. Sofo, J. V. Badding, and G. D. Mahan, Phys. Rev. B **68**, 085201 (2003).

[13] P. Larson, Phys. Rev. B **68**, 155121 (2003).

[14] T. Thonhauser, Solid State Commun. **129**, 249 (2004).

[15] M. Kim, A. J. Freeman, and C. B. Geller, Phys. Rev. B **72**, 035205 (2005).

[16] P. Larson, Phys. Rev. B **74**, 205113 (2006).

[17] S. Lee and P. von Allmenn, Appl. Phys. Lett. **88**, 022107 (2006).

[18] G. Wang and T. Cagin, Phys. Rev. B **76**, 075201 (2007).

[19]B.-L. Huang and M. Kaviany, Phys. Rev. B **77**, 125209 (2008).

[20]M. S. Park, J.-H. Song, J. E. Medvedeva, M. Kim, I. G. Kim, and A. J. Freeman, Phys. Rev. B **81**, 155211 (2010).

[21]S. V. Eremeev, Yu. M. Koroteev, and E. V. Chulkov, JETP Lett. **91**, 387 (2010).

[22]H. Li, D. Bilc, and S. D. Mahanti, Mat. Res. Soc. Symp. Proc. **793**, S8.37 (2003).

[23]*Numerical Data and Functional Relationship in Science and Technology*, edited by O. Madelung, M. Schulz, and H. Weiss, Landolt-Börnstein, New Series, Group III, Vol. 17f (Springer, New York, 1983); R. W. G. Wyckoff, *Crystal Structures 2*, (Wiley, New York, 1964); Th. L. Anderson, H. Krause, and H. Brigitte, Acta Crystallogr. B **30**, 1307 (1974).

[24]R. Zeller, P. H. Dederichs, B. Újfalussy, L. Szunyogh, and P. Weinberger, Phys. Rev. B **52**, 8807 (1995); N. Papanikolau, R. Zeller, and P. H. Dederichs, J. Phys. Condens. Matter **14**, 2799 (2002).

[25]S. H. Vosko, L. Wilk, and M. Nusair, Can. J. Phys. **58**, 1200 (1980).

[26]M. Gradhand, M. Czerner, D. V. Fedorov, P. Zahn, B. Yu. Yavorsky, L. Szunyogh, and I. Mertig, Phys. Rev. B **80**, 224413 (2009).

[27]J. M. Ziman, *Principles of the Theory of Solids* (Cambridge University Press, Cambridge, 1972).

[28]H. A. Ashworth, J. A. Rayne, and R. W. Ure, Phys. Rev. B **3**, 2646 (1972).

[29]We averaged the local relaxation time tensor of Ref. 28 over all equivalent extrema.

[30]P. Zahn, N. F. Hinsche, B. Yu. Yavorsky, and I. Mertig (unpublished).

[31]J. R. Drabble, R. D. Groves, and R. Wolfe, Proc. Phys. Soc. London **71**, 430 (1958); R. B. Mallinson, J. A. Rayne, and R. W. Ure Jr., Phys. Lett. **19**, 545 (1965).

[32]H. Schwarz, G. Björck, and O. Beckman, Solid State Commun. **5**, 905 (1967); V. A. Kulbachinskii, Z. M. Dashevskii, M. Inoue, M. Sasaki, H. Negishi, W. X. Gao, P. Lostak, J. Horak, and A. de Visser, Phys. Rev. B **52**, 10915 (1995).

[33]P. E. Blöchl, O. Jepsen, and O. K. Andersen, Phys. Rev. B **49**, 16223 (1994).